The large-scale organization of autonomous turbulent wall regions

By Javier Jiménez†, Oscar Flores‡ AND Manuel García–Villalba‡

1. Introduction

It has become clear in the last few years that wall-bounded turbulence below $y^+ \approx 80$ is a relatively autonomous system which not only functions in almost the normal way when the outer flow is artificially removed (Jiménez & Pinelli, 1999), but which is otherwise responsible for the generation of part of the turbulent energy dissipated in the outer flow regions (Jiménez, 1999). The structures in this near-wall layer scale approximately in wall units. None of this can of course be taken as proof that there is no interaction in natural wall turbulence between the inner and the outer layers, or that the inner layer is not modified by the presence of the core flow. It nevertheless suggests that any interaction is probably weak and affects only secondary aspects of the flow dynamics.

It has also been known for some time that there are structures in the outer flow which are very large, with lengths that scale at least in part with the boundary layer thickness (Perry, Henbest & Chong, 1986; Jiménez, 1998; Kim & Adrian, 1999). These structures contain most of the turbulent kinetic energy in the overlap region, and it is to be expected that their effect should be felt in some way by the near-wall structures (Hunt & Morrison 2000). Since the ratio between the boundary layer thickness, h, and the viscous wall length scale is the friction Reynolds number $Re_\tau = u_\tau h/\nu$, the outer structures become much larger than the near-wall ones as Re_τ increases. It can then be expected that any outer-inner interaction should include in that limit the large-scale organization of the near-wall layer.

The purpose of this paper is to explore that organization, and to attempt to clarify its origin. To that effect we will present numerical experiments in which the outer flow is effectively removed, and in which the scaling in wall variables should be strict. The nature of the interaction between the different layers will then be studied by comparing the large scales of these autonomous walls with those of full turbulent flows at various Reynolds numbers.

The organization of the paper is as follows. The numerical technique used to isolate the wall region is described in Section 2. The results, with special emphasis on the large-scale spectral characteristics of the isolated walls, are then discussed in Section 3 and compared with those of experimental and numerical full turbulent flows. Finally some conclusions are offered and opportunities for future work are explored.

2. The numerical experiments

The numerical scheme used for the autonomous simulations is similar to that described by Jiménez & Pinelli (1999) and by Jiménez & Simens (2001), but the method has been slightly modified, and the version described here should be preferred to those in the

† Also at U. Politécnica de Madrid
‡ U. Politécnica de Madrid

previous references. The Navier–Stokes equations are integrated in the form of evolution equations for the wall-normal vorticity ω_y and for $\phi = \nabla^2 v$, using a pseudospectral code with Fourier expansions in the two wall-parallel directions and Chebychev polynomials in y, as in Kim, Moin & Moser (1987). At each time step the right-hand sides of the two evolution equations are multiplied by a damping mask $1 - \Delta t\, F(y)$, where

$$F(y) = 0 \quad \text{if} \quad y \le \delta_1, \qquad F(y) = 1/T \quad \text{if} \quad y \ge \delta_2, \tag{2.1}$$

with the two limits connected smoothly by a cubic spline. Each time step can be written schematically as

$$\omega(t + \Delta t) = [\omega(t) + \Delta t N(t)][1 - \Delta t F(y)] \approx \omega(t) + \Delta t[N(t) - F(y)\omega(t)], \tag{2.2}$$

where ω stands for any of the two evolution variables, and N represents the full right-hand side of the Navier-Stokes equations. To the lowest order Eq. (2.2) is the discretization of

$$\partial_t \omega - N = -F(y)\omega. \tag{2.3}$$

In this interpretation the mask, where active, acts as a zeroth-order damping term for the evolution variables, both of which are related to the vorticity, and T is a damping time which is independent of the length scale of the fluctuations. In practice the time stepping is a third-order Runge-Kutta in which the masking filter is applied at each substep, and T has to be multiplied in Eq. (2.2) by $3/2$ to be consistent with Eq. (2.3). The Navier–Stokes equations are not modified at all below the mask lower limit δ_1.

When T is compared with the time λ^2/ν needed by molecular viscosity to damp a fluctuation of size λ, it defines a cut-off length scale $\lambda = (\nu T)^{1/2}$. Fluctuations shorter than this length are predominantly damped by viscosity, while longer ones are damped by the numerical mask. This scale is expressed in wall units as

$$\lambda^+ = T^{+\,1/2}. \tag{2.4}$$

In the experiments in this paper $T^+ \approx 1$, and all the fluctuations in the masked layer are essentially suppressed by the mask. While this is true for vorticity fluctuations, irrotational ones are not affected, and the outer edge of the Navier-Stokes layer is bounded by a potential core which prevents the formation of viscous boundary layers at the mask boundary.

While the flows in Jiménez & Pinelli (1999) and Jiménez & Simens (2001) were integrated at constant mass flux in a channel, the present experiments are carried at constant driving stress in a 'semi-infinite' domain. No-slip impermeable boundary conditions are imposed at $y = 0$, and the velocities are matched to the outer potential fluctuations at the edge of the computational domain, $y = 1$, using the method introduced by Corral & Jiménez (1995). The Chebychev polynomials of the wall-normal expansions are defined in a domain which is twice as high as the actual computational one, and only even or odd polynomials are used, depending on the variable to be represented. The mask height is adjusted so that the vorticities are essentially zero at the edge of this computational domain, so that their wall-normal spectral expansions remain accurate. The expansions of the variables which extend into the potential region, such as the velocities, are supplemented by exponentials. The coefficient of the $\exp[\mathrm{i}(\alpha x + \beta z)]$ Fourier component of the wall-normal velocity is, for example, expanded in terms of odd Chebychev polynomials plus the extra basis functions,

$$\exp[\pm(\alpha^2 + \beta^2)^{1/2} y], \tag{2.5}$$

which are homogeneous solutions of the Helmholtz equation satisfied by that particular Fourier mode as a consequence of incompressibility. Corral & Jiménez (1995) adjusted the coefficients of those extra functions to ensure the impermeability condition at $y = 0$ and the vanishing of the potential fluctuations as $y \to \infty$. The present code incorporates the extra freedom of substituting the condition at infinity by an impermeable slip boundary at $y = H > 1$, where the streamwise, wall-normal and spanwise velocity components, u, v and w, satisfy

$$v = 0, \qquad \partial_y u = \partial_y w = 0. \tag{2.6}$$

The limit $1/H \to 0$ recovers the semi-infinite domain discussed above.

The evolution equations for the (0, 0) Fourier modes of u and w cannot be expressed in terms of ω_y and ϕ, and are not modified by the numerical mask. Their expansions are also special. The exponentials are replaced by linear functions,

$$a_0 + b_0 y, \tag{2.7}$$

whose coefficients have to adjusted. Because there are no Reynolds stresses in the region where the mask is active, and because no mean pressure gradient is applied, the mean velocity profiles in the potential core are linear in y, with a slope b_0 that can be chosen arbitrarily (see Fig. 1*a*). The additive constant a_0 is then determined by the boundary condition at the wall. In our experiments the asymptotic slope of the profile of w is taken as zero, but that of u provides the driving force for the flow and determines the wall friction. All experiments in this paper are scaled so that the height of the computational domain is $y^+ = 120$. Note however that this height is irrelevant, because no turbulent flow extends above the mask height, which is always lower. The relevant turbulent Reynolds number is the height of the damping function $\delta_1^+ = u_\tau \delta_1 / \nu$, which determines the largest possible wall-normal size of the turbulent structures.

Since the goal of this paper is to study the large-scale organization of the wall, the simulations are carried out in computational boxes whose streamwise and spanwise periodicities are long, $L_x^+ \approx 10^4$, and wide, $L_z^+ \approx 10^3$. The resolution is in all cases $\Delta x^+ = 9$ and $\Delta z^+ = 5$ before dealiasing by the 2/3 rule, resulting in 1536×192 collocation points for the largest of the computational boxes discussed below. In the wall-normal direction, along which the expansion is not dealiased, 49 even or odd Chebychev modes are used. The first collocation point is at $y^+ = 0.06$.

3. Results

As already reported by Jiménez & Pinelli (1999), the turbulence statistics in these large autonomous boxes agree well with those of regular simulations in the unmasked layer, at least as long as $\delta_1^+ \gtrsim 50$. To avoid complications with marginal mask heights, all the experiments in this paper are run with $\delta_1^+ = 72$. Some of the resulting statistics are compared in Fig. 1 with the results for a complete channel at $Re_\tau = 550$ (del Álamo & Jiménez, 2001). The mean velocity shows a short 'logarithmic' layer before joining the linear profile of the irrotational region, while the velocity and vorticity fluctuations agree well with the results of the full channel up to about half the mask height. The peaks of the vorticity profiles located just above δ_1 are artifacts of the damping mask. They have already been described by Jiménez & Simens (2001), and are due to the reconnection of the vortex lines after they are truncated by the damping. The results for the other fluctuating quantities are similar to those included in the figure.

Our present concern is the spectral distribution of the turbulent energy among the

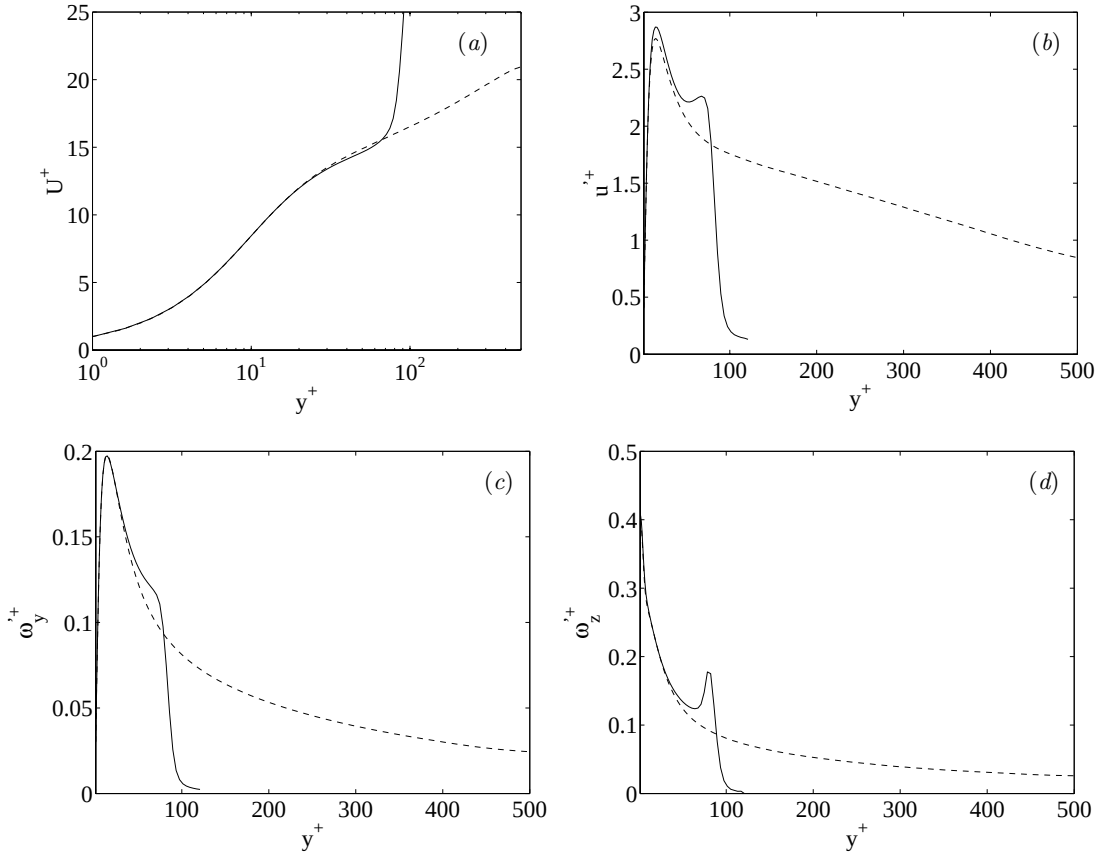

FIGURE 1. Mean profiles for: ——— , an autonomous wall $\delta_1^+ = 72$, $\delta_2^+ = 108$, $L_x^+ = 1.2 \times 10^4$, $L_z^+ = 10^3$, $1/H = 0$; - - - - , a complete channel, $Re_\tau = 550$, $L_x^+ = 1.4 \times 10^4$, $L_z^+ = 7 \times 10^3$. (a) Mean velocity. (b) Streamwise velocity fluctuations. (c) Wall-normal vorticity fluctuations. (c) Spanwise vorticity fluctuations.

different size ranges. It was shown by Jiménez & Pinelli (1999) that these autonomous flows contain structures which are visually indistinguishable from the velocity streaks and quasi-streamwise vortices found in the near-wall region of regular wall turbulence (Robinson 1991), and that they share with them their characteristic streamwise and spanwise length scales, $\lambda_x^+ \times \lambda_z^+ \approx 500 \times 100$, and their advection velocity $U_c^+ \approx 14$. Individual structures of similar sizes have been isolated by different methods in simplified Poiseuille flows (Jiménez & Moin 1991; Jiménez & Simens 2001; Waleffe 2001) and Couette flows (Nagata 1990; Waleffe 1998), and the intuitive reason for their scaling properties is that the presence of the wall constrains the wall-normal velocity fluctuations to sizes of the order of the wall distance.

On the other hand Townsend (1976) noted that no such constraint exists for the wall-parallel fluctuations, which can be larger. He named those hypothetical large structures 'inactive' because they could not, by themselves, create Reynolds stresses. We noted in the introduction that very large structures have indeed been identified and studied in the logarithmic layer. Hites (1997) measured the longitudinal velocity spectrum in boundary layers over a wide range of Reynolds numbers. He found that above $y^+ \approx 40$ the streamwise velocity spectrum is bimodal, with a shorter peak that scales in wall units

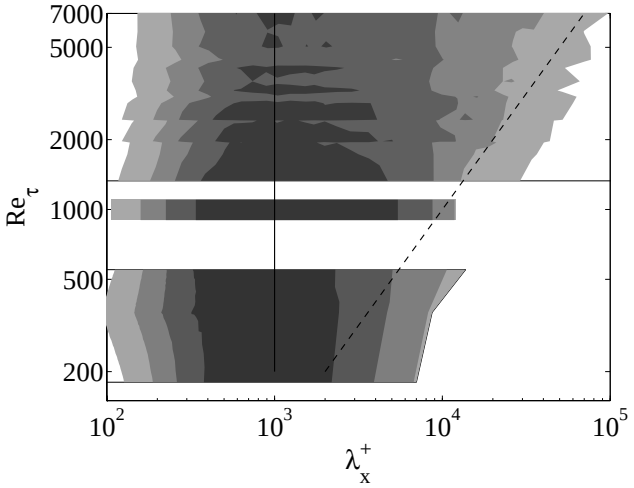

FIGURE 2. Longitudinal energy spectra for various near-wall flows. $y^+ = 20$. Gray levels correspond to the magnitude of $k_x E_{uu}$, as a function of the wavelength $\lambda_x = 2\pi/k_x$. Each line corresponds to a different Reynolds number. The upper block is interpolated from fifteen spectra of boundary layers (Hites, 1997). The lower one is interpolated from three numerical channels at $Re_\tau = 180$, 360 and 550 (del Álamo & Jiménez, 2001). The middle line is the autonomous wall computation in Fig. 1, whose Reynolds number has been assigned in a completely arbitrary manner. The dashed line is $\lambda_x = 10h$, where h is either the channel half-height or the boundary layer thickness, and the solid one is $\lambda_x^+ = 1000$.

and a longer one that scales in outer units, but he noted that the longer peak disappears below that height. His conclusions are strengthened by the comparison by Österlund *et al.* (2000) of the same data with spectra obtained on a different installation by a different group, as well as by the results obtained by Kim & Adrian (1999) in pipe flows above $y^+ = 100$. Older data to the same effect are summarized in Jiménez (1998). Most of those studies are restricted to the upper buffer layer and to the logarithmic layer, and do not emphasize the near-wall region.

More recently Metzger & Klewicki (2001) compared spectra at $y^+ = 15$ in two boundary layers with $Re_\theta = 2000$ and 5×10^6, and found a large excess of low-frequency energy in the latter with respect to the former. DeGraaff & Eaton (2000) made a comparative study of several boundary layers in a range of Reynolds numbers similar to those of Hites (1997). Although they did not measure spectra, they found that the intensity of the near-wall peak of the longitudinal velocity fluctuations, which is well inside the near-wall region, increases slowly with Reynolds number, again pointing to an effect of the outer flow on the wall layer.

In fact, a careful replotting of the available data very close to the wall confirms that the structures in this region are also subject to large-scale effects. This can be seen in Fig. 2 which shows longitudinal spectra of the streamwise velocity at $y^+ = 20$. The contour plot corresponds to individual premultiplied spectra which have been stacked together as a function of their Reynolds numbers, and which are treated as if they were a single function of Re_τ and of the streamwise wavelength $\lambda_x = 2\pi/k_x$. The upper block in the figure corresponds to the boundary layers in Hites (1997), while the lower one corresponds to three numerical channels by del Álamo & Jiménez (2001). The single spectrum between the two blocks will be discussed below.

It is clear that the long-wavelength end of the spectrum moves to the right as the Reynolds number increases, and that in the boundary layers it is approximately located at ten times the boundary layer thickness. The long-wavelength end of the channel spectra also lengthens with Reynolds number, but it does not seem to follow the same law. This disagreement is probably only apparent, and the spectra of the two highest-Reynolds number channels collapse fairly well with those of the boundary layers when the boundary layer thickness is defined as 2.5 times the channel half height. This is not unreasonable, since the outer part of the boundary layer, characterized by intermittent incursions of irrotational fluid, is missing from the channels, each of whose walls can roughly be described as the inner, fully-turbulent, part of a boundary layer. The main short-wavelength peak of the spectra remains relatively constant at $x^+ \approx 1000$ within this Reynolds numbers range.

Note that the large structures in the long-wavelength end of the spectra, with lengths of the order of $10^4 - 10^5$ wall units, are unlikely to be individual streaks. It is tempting to conclude that their origin is the distortion of the near-wall layer by the outer flow, which imposes on the wall its own large scales, but it is also possible that the wall organizes itself. Such self-organization is observed in many nonlinear systems, and it is of some interest to determine whether the near-wall large scales are autonomous or exogenous. Their expected behavior would be different in each case. If they were forced from outside it might, for example, be possible to control them by acting on the outer flow, while if the organization is self-induced such controls would probably be ineffective.

The question can be tested using the autonomous numerical simulations described in Section 2, since in them there are no outer structures with which the wall can interact. Figure 3 displays two-dimensional spectra from a numerical channel at $Re_\tau = 550$ (del Álamo & Jiménez, 2001), and from an autonomous wall with $\delta_1^+ = 72$. Both are computed in periodic boxes which are chosen to be as large as possible to minimize the interference of the computational domain with the large structures.

The first surprise is the almost perfect correspondence between the autonomous case and the fully-turbulent case, which strongly suggests that the large-scale organization of the wall regionis not due to the outer flow. There are no turbulent fluctuations above $y^+ \approx 80$ in the autonomous case. The agreement is specially good for the wall-normal component, for which the structures are relatively short and narrow. Their size more or less agrees with the individual vortex–streak structures isolated by Jiménez & Moin (1991). The second surprise is that the large structures of the streamwise velocity, and to a certain extent those of w, are actually *longer* in the autonomous wall than in the full channel. This also runs counter to the idea that the outer flow is the origin of the large near-wall scales.

The one-dimensional spectrum of u in the autonomous wall has been included in the compilation in Fig. 2 as the narrow line in the gap between the high-Reynolds number boundary layers and the channels. The Reynolds number assigned to it in the figure, $Re_\tau = 1000$, is completely arbitrary since, if any Reynolds number could be assigned to that flow, it would be the height $\delta_1^+ = 72$ of the numerical mask. The fact that this spectrum does not look out of place in its arbitrary location emphasizes that it is much longer than what could be expected from its thickness. The same conclusion can be drawn from the comparison of the one-dimensional spectra in Fig. 3(b).

The apparently contradictory observations that, on the one hand the large-scale structures are present in autonomous walls lacking an outer flow, while on the other hand they are limited in real boundary layers to lengths shorter than a fixed multiple of the

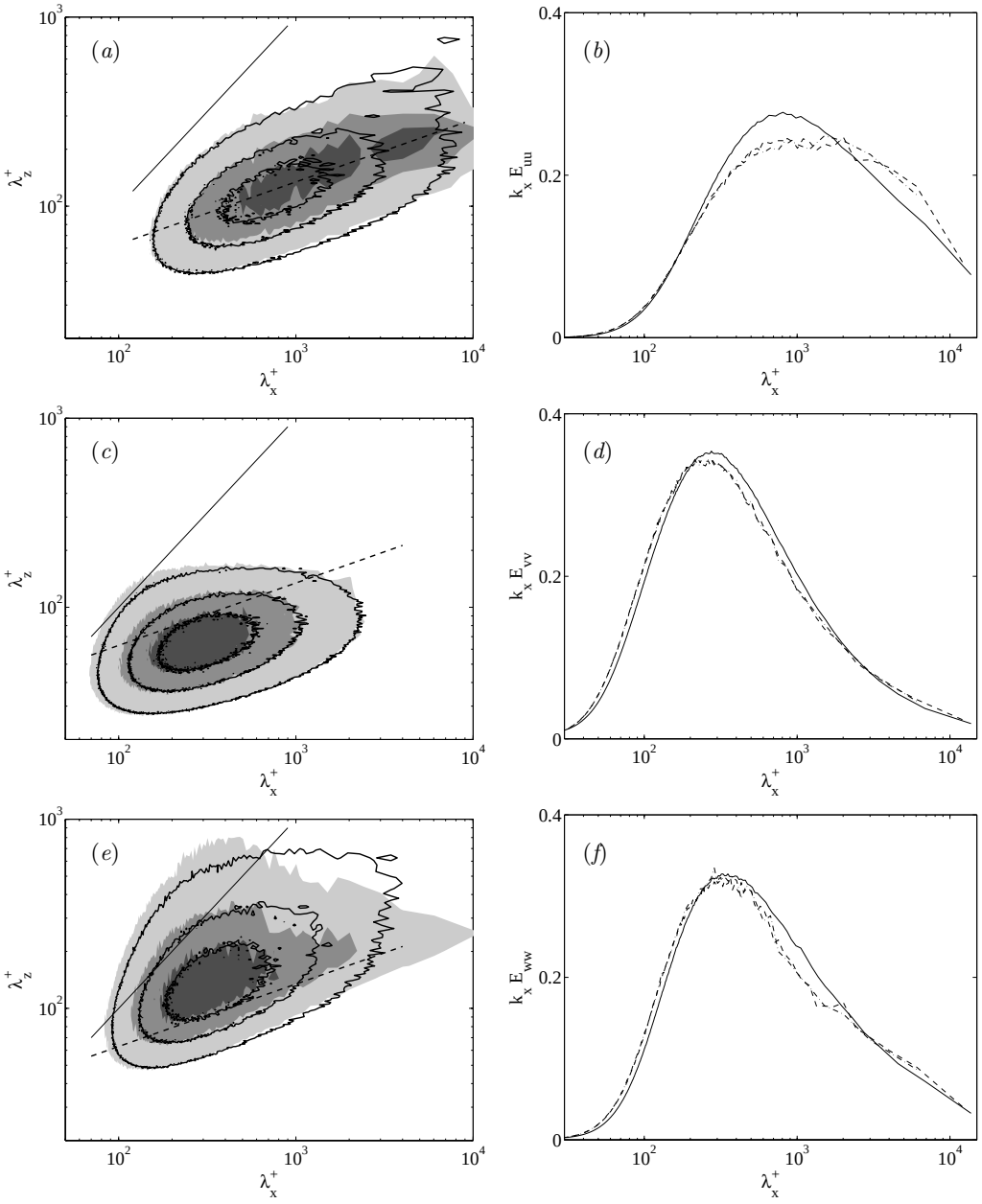

FIGURE 3. (*a*), (*c*), (*e*) Premultiplied two-dimensional velocity spectra, $k_x K_z E^{2D}(\lambda_x, \lambda_z)$, as functions of the streamwise and spanwise wavelengths. $y^+ = 16$. Shaded contours are the autonomous wall in Fig. 1. Lines are a full turbulent channel with $Re_\tau = 550$ (del Álamo & Jiménez, 2001). The solid lines are $\lambda_x = \lambda_z$, and correspond to horizontally isotropic structures. The dashed lines have logarithmic slopes 1/3, and pass through $\lambda_x^+ = \lambda_z^+ = 50$. The contours are (0.25, 0.5, 0.75) times the maximum value of each spectrum. (*b*), (*d*), (*f*) One-dimensional streamwise spectra, $k_x E(\lambda_x)$, for the same data. ——— , full channel; - - - - , the autonomous wall in Fig. 1. —·— , an autonomous wall with the same parameters except $L_x^+ = 6 \times 10^3$. (*a*), (*b*) Streamwise velocity. (*c*), (*d*) Wall-normal velocity. (*e*), (*f*) Spanwise velocity.

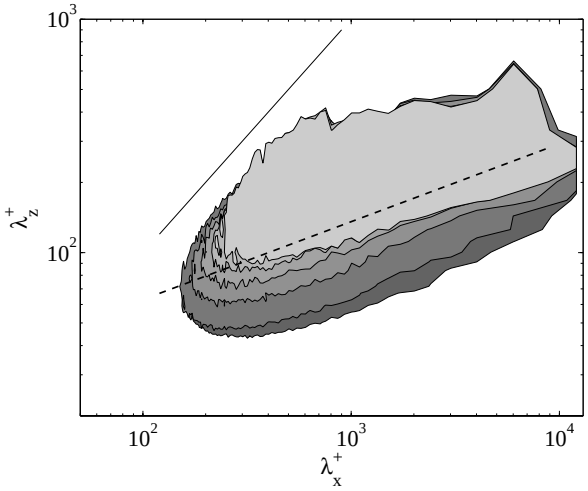

FIGURE 4. Each shaded contour is a premultiplied two-dimensional spectrum of the streamwise velocity at a different distance from the wall. From darker to lighter $y^+ = 10(10)60$. The flow is the autonomous wall in Fig. 1, and the contour values are the same as the outermost contour in Fig. 3. The length of the two axes correspond to the size of the computational box. The two trend lines are as in Fig. 3.

flow thickness, are best reconciled by assuming that the autonomous wall layer would by itself form infinitely long structures, and that the effect of the outer flow is to break those very long structures into pieces which are *shorter* than a given length. This is not as unlikely as it may seem, since the aspect ratio of the longest structures in Fig. 3(a) is already $L_x/y = 200$, and it is difficult to see how such a number might differ from infinity in terms of dynamics.

This raises the question of why the autonomous spectrum decreases sharply at its long-wave end in Fig. 3(b). In other words, why it is not really infinitely long. Part of the answer might be the interference of the finite size of the box, since the decrease appears only in the second longest numerical harmonic, which is probably strongly influenced by the finite domain. This possibility is reinforced by the behavior of the autonomous spectra farther from the wall. The good correspondence with the spectra of the full flows is maintained up to $y^+ \approx 40$, but higher up the autonomous box is both too short and in particular too narrow to contain its own structures. This is seen in Fig. 4 which shows spectra as a function of wall distance. The highest level in that figure is already close to the numerical mask, at it is clear that it is constrained at it widest point by the width of the box. It is plausible to suppose that one result of that constriction might be to limit the extent of the spectra everywhere. On the other hand, an attempt to reproduce that effect using shorter numerical boxes did not produce clear results. The right-hand side of Fig. 3 contains spectra from two autonomous simulations, in addition to those from the full channel. The results discussed up to now have been those from the longest autonomous box, but the figure also shows another set of spectra from a box of the same width, but only half as long. They are difficult to distinguish from those in the longer box and, in particular, the E_{uu} spectrum in the shorter box does not show a sharp drop in its longest harmonic comparable to that in the longer box. More work is needed before the effect of box size is clarified, and more extensive simulations are in progress.

It is clear from Fig. 3 that the longer scales are also wider, and that this part of the

flow is far from being isotropic. This is specially true of the longitudinal velocity, and it is interesting that the 'ridge' in that spectrum follows fairly closely the power law

$$\lambda_x \sim \lambda_z^3. \tag{3.1}$$

It is dangerous to extrapolate similarity laws from limited experimental data without a plausible theoretical model, but del Álamo & Jiménez (2001) found the same power law in complete channels near the wall, giving some support to the idea that the relation might be real. The spectra of the other two velocity components are closer to being isotropic.

Del Álamo & Jiménez (2001) show that, in the logarithmic layer of complete wall-bounded flows, the two-dimensional spectra satisfy a different power law

$$\lambda_x \sim \lambda_z^2, \tag{3.2}$$

and they speculate that it may be related to the downstream spreading of perturbations induced on the mean velocity profile by localized transverse velocities. In essence they propose that Eq. (3.2) is a reflection of the form of the similarity solutions of the diffusion-advection equation,

$$\partial_x u = (\partial_{yy} + \partial_{zz})u, \tag{3.3}$$

which take the form

$$u = x^{-1}\widehat{u}(y/x^{1/2},\, z/x^{1/2}). \tag{3.4}$$

The relation Eq. (3.2) would derive from the form of the spanwise similarity variable in Eq. (3.4).

A similar argument can be used to support Eq. (3.1). Near the wall the mean flow velocity is closer to a pure shear than to the approximately- constant velocity of the logarithmic layer. The diffusion equation then takes the form

$$y\partial_x u = (\partial_{yy} + \partial_{zz})u, \tag{3.5}$$

whose similarity solutions are

$$u = x^{-1}\widehat{u}(y/x^{1/3},\, z/x^{1/3}), \tag{3.6}$$

leading to Eq. (3.1). Note that these arguments can only be treated as indicative, since the diffusion at the scale of these large structures is probably due to smaller-scale turbulence, while both Eq. (3.3) and Eq. (3.5) assume a constant eddy viscosity.

4. Conclusions

We have shown that the self-sustaining small-scale structures of the near-wall region are able to organize themselves into much larger scales, especially visible in the spectra of the streamwise velocity component. In the absence of any outer flow the length of these large structures appears to be infinite, at least within the limits of the present numerical simulations, but in actual turbulent flows they scale as multiples of the flow thickness. We have suggested that this interaction takes the form of a shortening of the near-wall structures by the random perturbations originating in the outer flow.

The precise mechanism of this interaction is not clear from the present experiment. The numerical parameter H at which the slip boundary condition (2.6) is applied was introduced for this purpose, on the assumption that the postulated infinite length of the structures in the autonomous simulations was a reflection of the infinite distance

at which the irrotational boundary condition was applied. An autonomous box was run using $H = 2$, which corresponds to a slip wall at $y^+ = 240$ but, while the spectra shortened a little, the effect was too weak to be considered as a model for the interaction in real flows. Presumably the rotational fluctuations of the turbulent core flows are more effective in disturbing the wall that the irrotational fluctuations in our model.

We have shown that the width of the near-wall large structures scales like the cube root of their length, and we have proposed a simple scaling explanation for that power law. The assumption is that the large u-structures are the dissipating wakes of the perturbations introduced in the mean profile by occasional small-scale sweeps or ejections. The essence of this argument is that the large scales, being very anisotropic and therefore subject to very different time scales in their transverse and longitudinal directions, can be modelled as linear objects which only see the small-scale turbulence as either an eddy viscosity or as a random forcing. If this is true, it should possible to derive quantitative predictions on their spectra from the properties of some modified Orr-Sommerfeld or Squires equation.

This work was supported in part by the Spanish CICYT contract BFM2000-1468 and by ONR grant N0014-00-1-0146. O.F. and M.G-V. were supported in part by undergraduate fellowships from the Universidad Politécnica of Madrid. We are grateful to J.C. del Álamo and P. Bradshaw for reading an early version of the manuscript and providing useful suggestions.

REFERENCES

Corral, R. & Jiménez, J. 1995 Fourier/Chebyshev methods for the incompressible Navier Stokes equations in infinite domains, *J. Comput. Phys.* **121**, 261–270.

DeGraaff, D.B. & Eaton, J.K. 2000 Reynolds number scaling of the flat-plate turbulent boundary layer, *J. Fluid Mech.* **422**, 319–346.

Del Álamo, J.C. & Jiménez, J. 2001 Direct numerical simulation of the very-large anisotropic scales in a turbulent channel. *Annual Research Briefs*, Center for Turbulence Research, NASA Ames/Stanford Univ., 329–341.

Hites, M.M. 1997 Scaling of high-Reynolds number turbulent boundary layers in the National Diagnostic Facility. *Ph. D. Thesis* Illinois Inst. of Technology.

Hunt, J.C.R. & Morrison, J.F. 2000 Eddy structures in turbulent boundary layers. *Eur. J. Mech. B - Fluids* **19**, 673–694.

Jiménez, J. 1999 The physics of wall turbulence, *Physica* A **263**, 252–262.

Jiménez, J. 1998 The largest scales of turbulent wall flows. In *CTR Ann. Res. Briefs*, Stanford Univ. 137–154.

Jiménez, J. & Moin, P. 1991 The minimal flow unit in near wall turbulence. *J. Fluid Mech.* **225**, 221–240.

Jiménez, J. & Pinelli A. 1999 The autonomous cycle of near wall turbulence, *J. Fluid Mech.* **389**, 335–359.

Jiménez, J. & Simens, M.P. 2001 Low-dimensional dynamics in a turbulent wall, *J. Fluid Mech.*, **435**, 81–91.

Kim, K.C. & Adrian, R.J. 1999 Very large-scale motion in the outer layer. *Phys. Fluids* **11**, 417–422.

Kim, H.T., Kline, S.J. & Reynolds, W.C. 1971 The production of turbulence near a smooth wall in a turbulent boundary layers. *J. Fluid Mech.* **50**, 133-160.

Kim, J., Moin, P. & Moser, R. 1987 Turbulence statistics in fully developed channel flow at low Reynolds number. *J. Fluid Mech.* **177**, 133–166.

Metzger, M.M. & Klewicki, J.C. 2001 A comparative study of near-wall turbulence in high and low Reynolds numbers boundary layer, *Phys. Fluids* **13**, 692–701.

Moser, R., Kim, J. & Mansour, N.N. 1999 Direct numerical simulation of a turbulent channel flow up to $Re_\tau = 590$. *Phys. Fluids* **11**, 943–945.

Nagata, M. 1990 Three-dimensional finite-amplitude solutions in plane Couette flow: bifurcation from infinity. *J. Fluid Mech.* **217**, 519–527.

Österlund, J.M., Johansson, A.V., Nagib, H.M. & Hites, M.H. 2000 Spectral characteristics of the overlap region in turbulent boundary layers. Extended abstract for *Int. Congr. Theor. Appl. Math. 2000*, Chicago.

Perry, A. E., Henbest, S. & Chong, M. S. 1986 A theoretical and experimental study of wall turbulence. *J. Fluid Mech* **165**, 163–199.

Robinson, S.K. 1991 Coherent motions in the turbulent boundary layer. *Ann. Rev. Fluid Mech.* **23**, 601–639.

Townsend, A.A. 1976 *The Structure of Turbulent Shear Flow*. Cambridge Univ. Press, 2nd. ed., p. 135.

Waleffe, F. 1998 Three-dimensional coherent states in plane shear flows. *Phys. Rev. Letters* **81**, 4140–4143.

Waleffe, F. 2001 Exact coherent structures in channel flow. *J. Fluid Mech.* **435**, 93–102.